Acta Oceanol. Sin., 2019, Vol. 38, No. 4, P. 175–182
https://doi.org/10.1007/s13131-019-1421-7
http://www.hyxb.org.cn
E-mail: hyxbe@263.net

Sectional characteristics of temperature, salinity and density off the central Zhejiang coast in the spring of 2016

Longqi Yang[1], Zhaozhang Chen[1]*, Zhenyu Sun[1], Jianyu Hu[1]

[1] State Key Laboratory of Marine Environmental Science, College of Ocean and Earth Sciences, Xiamen University, Xiamen 361102, China

Received 9 February 2018; accepted 27 April 2018

Abstract

In this study, the sectional characteristics of temperature, salinity and density off the central Zhejiang coast were analyzed using three sections of observational data in the spring of 2016. The results are as follows: (1) a cold water patch was observed in the middle layer of sections from 10 to 25 m, and a weak upwelling was observed at the upper layer near the central Zhejiang coast; (2) several thermoclines, inverted thermoclines, and haloclines were observed in the survey area; (3) the Taiwan Warm Current Water (TWCW) climbing from the slope towards the survey area affected the thermocline, making it thinner and intensified; however, the TWCW was not strong enough to break through the thermocline to reach the sea surface.

Key words: temperature, salinity, Taiwan Warm Current Water, central Zhejiang coast

Citation: Yang Longqi, Chen Zhaozhang, Sun Zhenyu, Hu Jianyu. 2019. Sectional characteristics of temperature, salinity and density off the central Zhejiang coast in the spring of 2016. Acta Oceanologica Sinica, 38(4): 175–182, doi: 10.1007/s13131-019-1421-7

1 Introduction

The Zhejiang coast is located on the continental shelf of the East China Sea. It is affected by the northeasterly monsoon in winter and southeasterly monsoon in summer. The coast is also affected by the terrain, the Changjiang Diluted Water, the Zhe-Min Coastal Water, and the Taiwan Warm Current Water (TWCW). The Zhe-Min Coastal Water flows southwestward in winter. However, Qiao (2012) reported that the direction of the Zhe-Min Coastal Water has a larger change in May than in winter, i.e., it still flows southwestward as a coastal current in the sea area north of 28°N, whereas it turns northeastward in the sea area south of 28°N. The TWCW with a high temperature and high salinity is located outside the Zhe-Min Coastal Water and flows northeastward all year round. In the sea area south of 29°N and west of 123°E, it flows along 50 m and 100 m isobaths. These lead to diverse hydrological characteristics in this area.

The Zhejiang coast is also an area of typical upwelling (Hu and Wang, 2016). Upwelling has a key influence on the nutrient transport and ecological environment of the Zhejiang fishery, making this area more complex (Tang et al., 2006; Yang et al., 2013; Wang et al., 2014; Wu et al., 2015; Song et al., 2017). For decades, many researchers have studied the hydrological characteristics of the sea area by analyzing the temperature, salinity and density distributions and discussed the variability and mechanisms of upwelling (Mao et al., 1963; Hu et al., 1980; Pu, 1983; Pan et al., 1985; Beardsley et al., 1985; Xu, 1986). In recent years, many satellite, shipboard, and moored observations have been carried out to further analyze these problems (Zhou et al., 2009; Lou et al., 2011; Zeng et al., 2012; Shi et al., 2013; Li et al., 2014; Zhang et al., 2014; Xu et al., 2015). Numerical models have also been established to elucidate the mechanisms of these phenomena (Liu and Su, 1991; Luo et al., 1998; Huang et al., 1996; Pan and Sha, 2004; Qiao et al., 2006; Lü et al., 2006, 2007; Bai et al., 2009). However, there are still large differences among these observational and numerical results.

Hu et al. (1980) and Huang (1996) believed that the interaction between topography and the TWCW is the primary cause of the upwelling off the Zhejiang coast. Some researchers assumed that the wind force and topography both contribute to the upwelling in Zhejiang coastal waters (Pan et al., 1985; Luo et al., 1998). Zhu (2003) studied the upwelling by a numerical model and proposed that mainly the barotropic effect accounts for upwelling. Qiao et al. (2006) and Lü et al. (2006) proposed the combination of topography and strong tidal mixing to elucidate the mechanism of upwelling. However, most studies in this area focused on summertime, because the distributions of physical parameters can be easily identified, such as the sea surface temperature. Studies of spring cases are relatively rare (Ni et al., 2014).

2 Data

To study the characteristics of temperature, salinity and density off the central Zhejiang coast in spring, a survey was carried out from April 30, 2016 to May 14, 2016. The surveyed sea area and stations off the central Zhejiang coast are shown in Fig. 1. There are mainly three sections with 25 stations. Section A is located near Ningbo City. Section B is located near Xiangshan County, and Section C is located near Taizhou City. During the survey, an SBE 917 instrument from the Sea Bird Company was used to acquire the data profiles of temperature and salinity. The

Foundation item: The National Key R&D Program of China under contract No. 2018YFC1406302; the National Basic Research Program of China under contract No. 2015CB954004; the National Natural Science Foundation of China under contract Nos 41230961, U1405233 and 41776027.

*Corresponding author, E-mail: zzchen@xmu.edu.cn

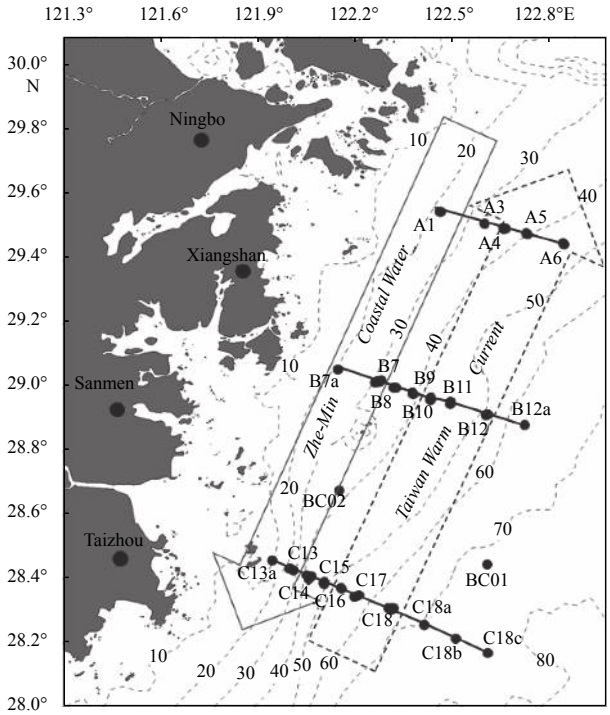

Fig. 1. Observation stations during the survey in the spring of 2016. The dashed contour lines show the depth with a contour interval of 10 m. The solid and dashed arrows show the Zhe-Min Coastal Water and the inshore branch of TWCW, respectively (redrawn from Qiao (2012)).

precision of temperature was 0.001°C, and the precision of conductivity was 0.000 3 S/m. Several observations along the same section were carried out during this survey; they can be used to analyze the variational characteristics of temperature and salinity over a short period.

We also used the daily wind field data from satellite remote sensing. The data were obtained from ASCAT (Advanced Scatterometer; ftp.ifremer.fr/ifremer/cersat/products/gridded/). The resolution of this product was (1/4)°×(1/4)° (http://apdrc.soest.hawaii.edu/doc/ascat_doc.pdf).

3 Results

Figure 2 shows the distributions of temperature, salinity and density along Section A on May 8, 2016. The temperature first decreases and then increases from the surface to the bottom in Section A, and a cold water patch exists in the middle layer located from 10 to 25 m. Such a "middle layer cold water" was also observed by Xu et al. (2000). The salinity in Section A increases with depth. The high temperature (>17°C), low salinity (<31) and low density (<21 kg/m^3) water in the upper layer is regarded as the Zhe-Min Coastal Water. The high temperature (>17°C), high salinity (>33), and high density (>24 kg/m^3) water in the lower layer is the inshore branch of TWCW. Figure 2 also shows the TWCW climbing between Stas A3 and A5. In addition, thermoclines are present between two water masses. For example, at Sta. A4, a thermocline with an intensity of 0.51°C/m appears from 7 to 10 m (Fig. 3a); a weak inverted thermocline with an intensity of 0.29°C/m appears from 17 to 19 m; a halocline with an intensity of 0.64 m^{-1} appears from 13 to 20 m in Section A.

Figure 4 shows the distributions of temperature, salinity and density on May 4, 6, 9, and 12 in Section B. The stratification of temperature or salinity in Section B is very clear. A cold water patch was also observed in the middle layer from 10 to 25 m in Section B. The Zhe-Min Coastal Water in the upper layer and the TWCW in the lower layer are also distributed in Section B. On May 4, a thermohaline appeared from 5 to 8 m at Sta. B9. The 18°C isotherm and 29 isohaline were upwards, as were the 17°C isotherm and 34 isohaline in the lower layer. These indicate an upwelling formation in the upper layer and the TWCW climbing in the lower layer. On May 6, the upwelling in the upper layer outcropped to the sea surface and the climbing of TWCW was stronger than before. On May 9, the upwelling in the upper layer of Section B disappeared. The climbing of TWCW in the lower layer of Section B was still very clear. However, the strength of climbing seemed to be weaker than that on May 6. On May 12, the mixing layer thickened, and the climbing of TWCW was not clear. Regarding the density distribution in Section B, the 20 isopycnal was convex and outcropped to the sea surface on May 4 and 6. On May 6 and 9, the climbing high density water was evident. On May 12, the climbing phenomenon disappeared in the lower layer.

Table 1 shows the variations in the depth and intensity of

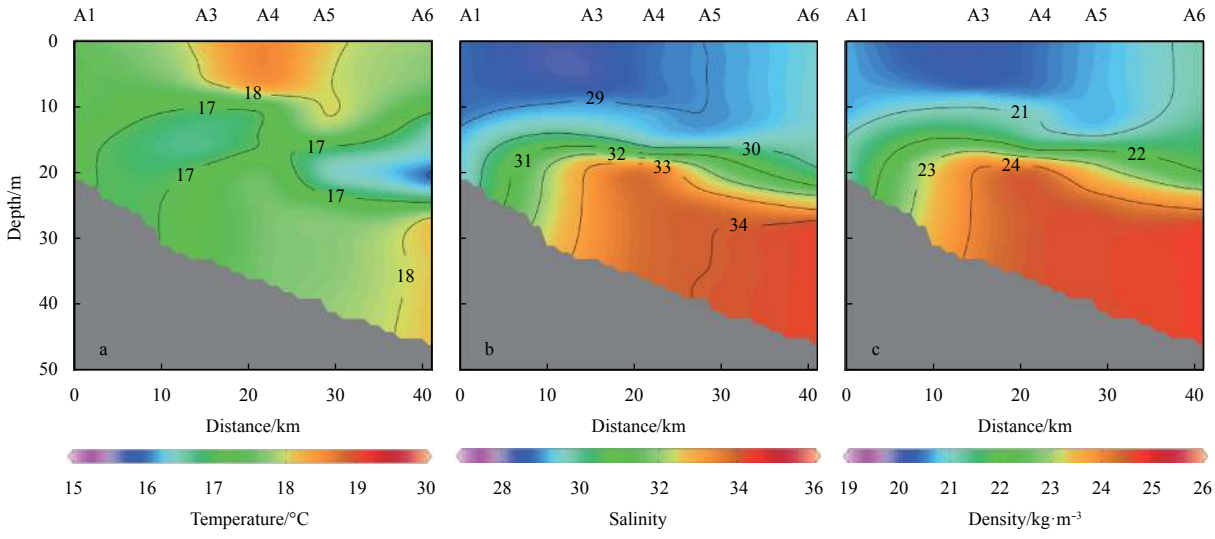

Fig. 2. Distributions of temperature (a), salinity (b), and density (c) along Section A on May 8, 2016.

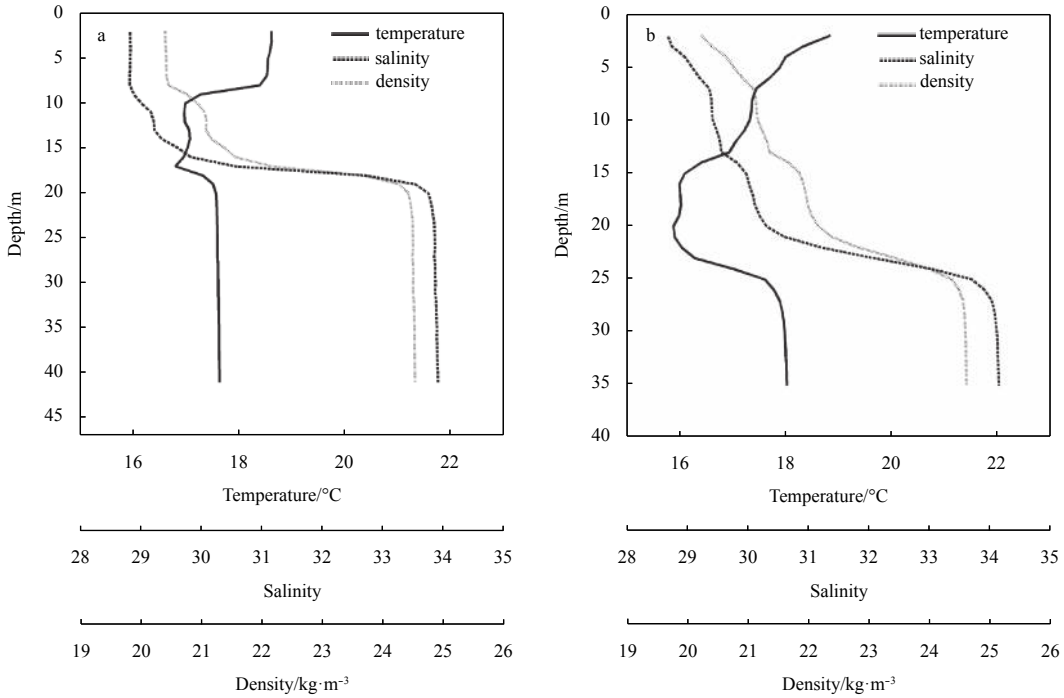

Fig. 3. Vertical distributions of temperature, salinity and density at Sta. A4 on May 8 (a) and at Sta. B9 on May 4, 2016 (b).

thermocline and inverted thermocline at Sta. B9. The inverted thermocline in Table 1 is shown as a negative value. As a whole, the intensity, thickness, and depth of thermocline and inverted thermocline were different at each measurement. They can be roughly divided into upper thermocline, middle thermocline, and lower inverted thermocline. A weak upper thermocline appeared between 2 and 7 m at Sta. B9, and the intensity was 0.27°C/m on May 4 (Fig. 3b). This can be attributed to the effect of upwelling (Fig. 4). On May 6, this thermocline disappeared. This is because the thermocline was broken by upwelling outcropped to the sea surface (Fig. 4). From May 4 to May 6 and then to May 9, the middle thermocline thickness increased from 2 to 5 m and then decreased to 2 m. The intensity of thermocline was between 0.38–0.40°C/m. On May 12, the thickness was still 2 m; however, the intensity decreased to 0.30°C/m. In the inverted thermocline, from May 4 to May 6, the depth increased and the thickness remained unchanged, and the intensity ranged from –0.43 to –0.57°C/m. On May 9, the intensity decreased to –0.37°C/m. Finally, on May 12, the inverted thermocline disappeared. From May 4 to May 6, the climbing of the TWCW increased as the intensity of inverted thermocline increased. On May 9, the climbing of TWCW decreased; therefore, the intensity of inverted thermocline decreased. On May 12, the phenomenon of TWCW climbing disappeared, and the inverted thermocline also disappeared. It can be concluded that the intensity of inverted thermocline had a good correspondence with the climbing of TWCW.

Table 2 shows variations in the depth and intensity of halocline at Sta. B9. As shown in Table 2, a weak halocline appeared between 3 to 7 m, and the intensity of halocline was 0.15 m^{-1} on May 4 (Fig. 4b). On May 6, the upper halocline disappeared owing to the effect of upwelling. As shown in Table 2, the middle layer (15–19 m) showed two haloclines on May 4. Then, the two haloclines merged into one large halocline on May 6, because of the climbing of TWCW. On May 9, the big halocline divided into two small haloclines again, but the depth of haloclines slightly increased. On May 12, the depth of halocline clearly increased. The thickness increased, but the intensity decreased.

Based on the analysis shown in Tables 1 and 2, it can be concluded that both the strength of upwelling and intensity of TWCW climbing affect the depth, thickness, and intensity of thermocline or halocline layer. When the upwelling and climbing are strengthened, the depth of thermocline or halocline layer decreases, the thickness decreases, and the intensity increases; otherwise, the reverse occurs. However, notably the effect is not absolute. Upwelling is only one of the factors affecting the thermocline or halocline layer. For example, from May 6 to May 9, the intensity of TWCW climbing slightly weakened, whereas the thickness of inverted thermocline slightly decreased despite the decrease in intensity.

Figure 5 shows the distributions of temperature, salinity, and density in Section C. Distributions in Section C are similar to those in Sections A and B, but there are some differences among them. Based on the temperature distribution in Section C on May 3, in the upper layer, the 18°C and 19°C isotherms between Stas C16 and C18 were upward and convex. The 29 and 30 isohalines were clearly lifted. The cold water below 17°C in the middle layer was distributed between 8 and 40 m to the west of Sta. C17. On May 3, several thermoclines, inverted thermoclines, and haloclines appeared at Section C. Taking Sta. C15 as an example, three thermoclines existed from 4 to 6 m, from 9 to 15 m, and from 20 to 22 m. The intensities of these thermoclines were 0.22, 0.28 and 0.58°C/m, respectively. Two inverted thermoclines existed from 16 to 18 m and from 26 to 30 m; the intensities of these inverted thermoclines were –0.30 and –0.51°C/m, respectively. On May 3, two haloclines existed from 4 to 19 m and from 22 to 30 m; the intensities of these haloclines were 0.15 and 0.31 m^{-1}, respectively. Compared with the observations on May 3, a high-temperature water tongue appeared to the east of Sta. C18a from 20 to 50 m on May 11. This first decreased the temperature from

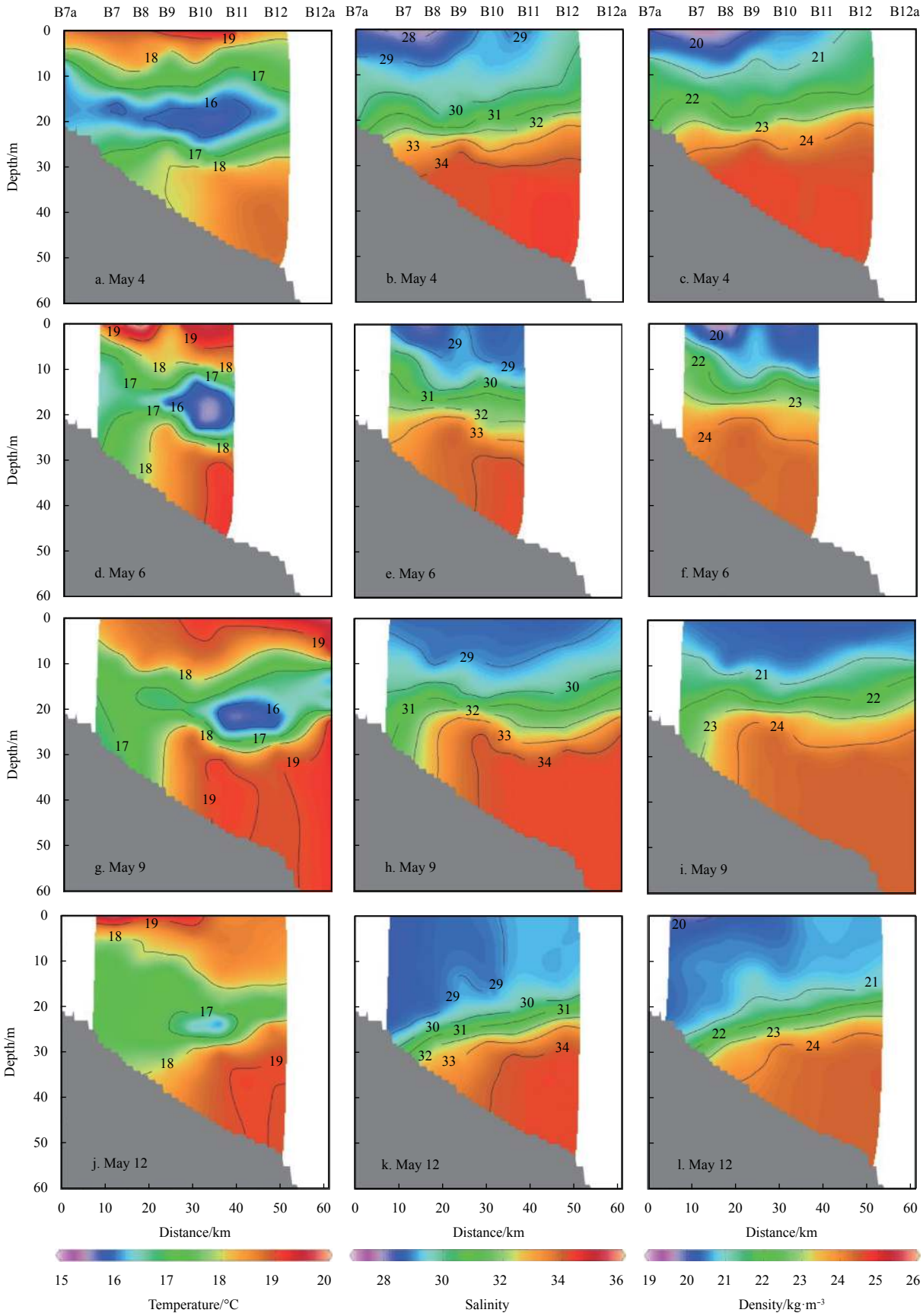

Fig. 4. Distributions of temperature (left), salinity (middle), and density (right) on May 4, May 6, May 9, and May 12 in Section B.

Table 1. Variations in depth and intensity of thermocline at Sta. B9

May 4		May 6		May 9		May 12	
Depth/m	Intensity/°C·m^{-1}	Depth/m	Intensity/°C·m^{-1}	Depth/m	Intensity/°C·m^{-1}	Depth/m	Intensity/°C·m^{-1}
2–7	0.27						
13–15	0.40	12–17	0.38	10–12	0.39	10–12	0.30
22–26	–0.43	18–22	–0.57	19–21	–0.37		

Note: The intensity with a negative value indicates inverted thermocline.

Table 2. Variations in depth and intensity of halocline at Sta. B9

May 4		May 6		May 9		May 12	
Depth/m	Intensity/m^{-1}	Depthm	Intensity/m^{-1}	Depth/m	Intensity/m^{-1}	Depth/m	Intensity/m^{-1}
3–7	0.15						
13–15	0.19	11–23	0.38	10–14	0.20	18–34	0.27
19–27	0.48			16-25	0.39		

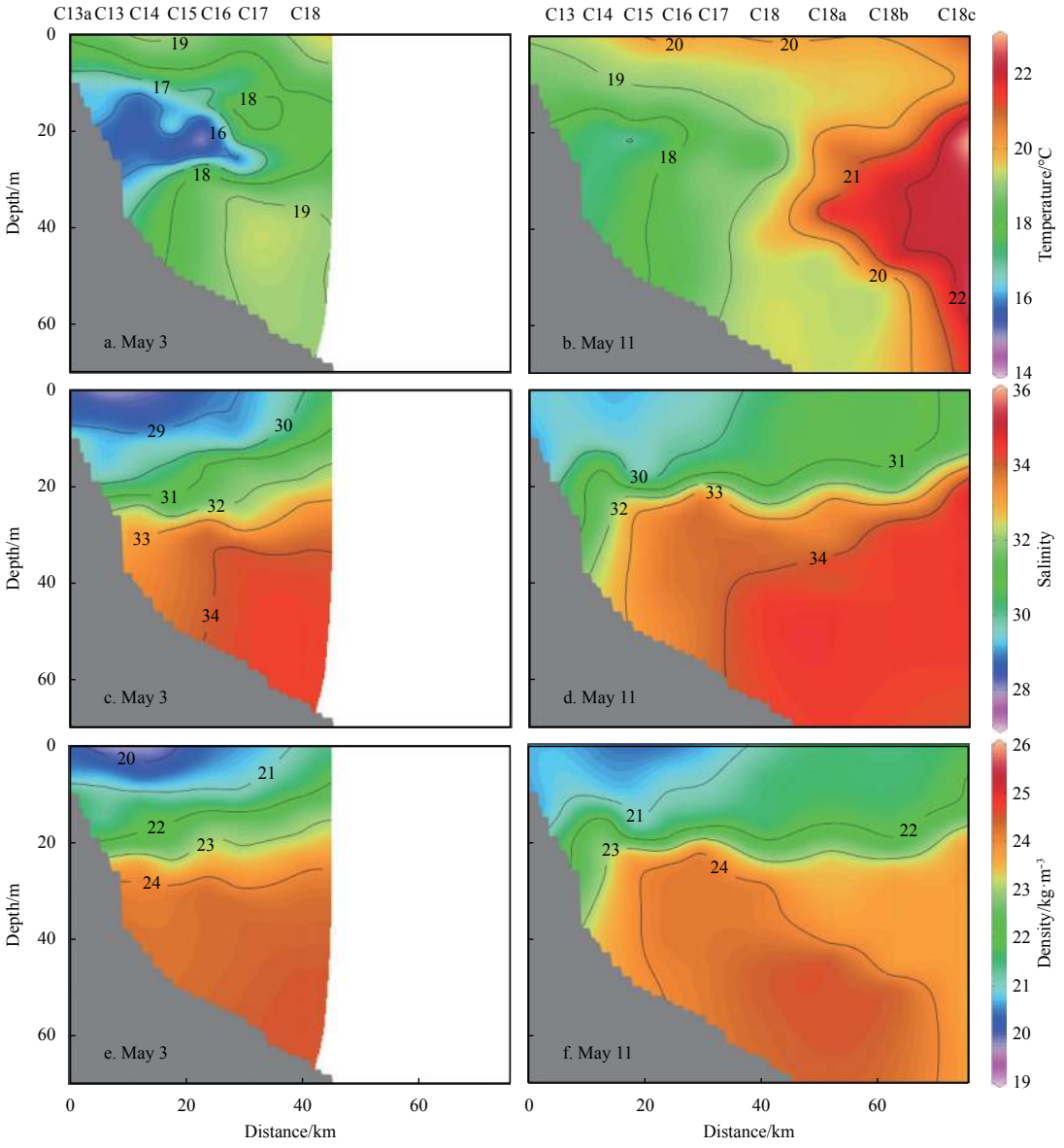

Fig. 5. Distributions of temperature (upper), salinity (middle), and density (lower) in Section C. On the left is the observation on May 3, and on the right is the observation on May 11.

the top to the bottom, then increased, and then decreased again. To the west of Sta. C17, the area of cold water in the middle layer decreased much more. The 29 isohaline disappeared on May 11, and the 33 isohaline of the lower layer was upward. However, the

34 isohaline did not show a similar feature. The intensity of high-density water climbing in the lower layer was very strong. On May 11, the number of thermocline or halocline clearly decreased. A thermocline formed from 18 to 21 m with an intensity of 0.46°C/m and a strong halocline formed from 18 to 25 m with an intensity of 0.44 m^{-1}.

4 Discussion

This study found cold water patches in the middle layer distributed from 10 to 25 m through temperature distributions in the three sections. This is an important marine phenomenon along the central Zhejiang coast in spring. Cold water patches appear where the isopycnals are dense (or at the thermocline). Owing to the buoyancy effect, the cold water is above the high-density water. In spring, both the surface heat content and bottom temperature of TWCW increase. This is an important factor to keep the cold water patch in the middle layer. There are two possible sources of cold water: (1) The local winter surface water (mixed water from the southern Yellow Sea surface water and East China Sea surface water) extends downward as the water is cooled. (2) The Zhe-Min Coastal Water sinks and expands eastward in winter (Wang et al., 2002).

The thermohaline characteristics of the three sections showed upwelling and TWCW climbing. Upwelling is induced by wind, tide, topography, and background flow (Hu and Wang, 2016). Ni et al. (2014) also showed that wind, TWCW, and tide are important factors affecting the upwelling of Zhejiang coastal sea in spring.

To establish the relationship between upwelling and wind, variation in daily wind speed, wind direction, thermohaline of 3 m layer (significantly affected by upwelling), and thermohaline of 22 m layer (significantly affected by the climbing of TWCW) at Sta. B9 were investigated. From May 1 to May 6, a southerly wind was dominant, as shown in Fig. 6a (also see Figs 7a and b). After May 6, a northerly wind was dominant and strongest on May 7 (also see Figs 7c and d). Figure 6b shows that the 3 m layer has the characteristics of low temperature and high salinity in the early period (from May 4 to May 6) and high temperature and low salinity in the late period (from May 9 to May 12). On May 6, the 3 m layer had a minimum temperature and maximum salinity. At the time of observation, the upwelling was the strongest (Fig. 4). From May 6 to May 9, the temperature increased rapidly, and the salinity decreased rapidly in the 3 m layer. After May 9, the temperature and salinity in the 3 m layer changed only slightly. Analysis of Fig. 6a shows a continuous southerly wind before May 6, resulting in the strongest upwelling on May 6. After May 6, the southerly wind quickly turned into a strong northerly wind, causing the upwelling disappear.

Figure 6c shows that the temperature and salinity of the 22 m layer first increased and then decreased. This reflects the strength of TWCW, and this first increases and then decreases. The temperature and salinity of the 22 m layer slightly decreased on May 9 (Fig. 6c); however, the climbing was still quite remarkable (Figs 4e and f). After May 9, the temperature and salinity of the 22 m layer significantly decreased (Fig. 6c). Combining Figs 6a and c, it was found that the southerly wind between May 4 and May 6 was accompanied by an enhanced TWCW climbing. The climbing was still quite remarkable on May 9, even though the southerly wind had turned into a strong northerly wind on May 7 and later. Notably, still a significant phenomenon of climbing was observed in Section A on May 8, even though the strong northerly wind still existed the day before. Some previous studies also showed that the TWCW climbing is inconsistent with the wind. For example, Pan et al. (1985) analyzed the observational data of State Oceanic Administration along 29°N in June 1977 and June 1978 and noted that the TWCW still climbed despite the disadvantageous condition of east-northeasterly wind. The analysis of other data of winter 1982 showed that even though the northeasterly wind prevailed, the bottom area still had a climbing shoreward component of flow.

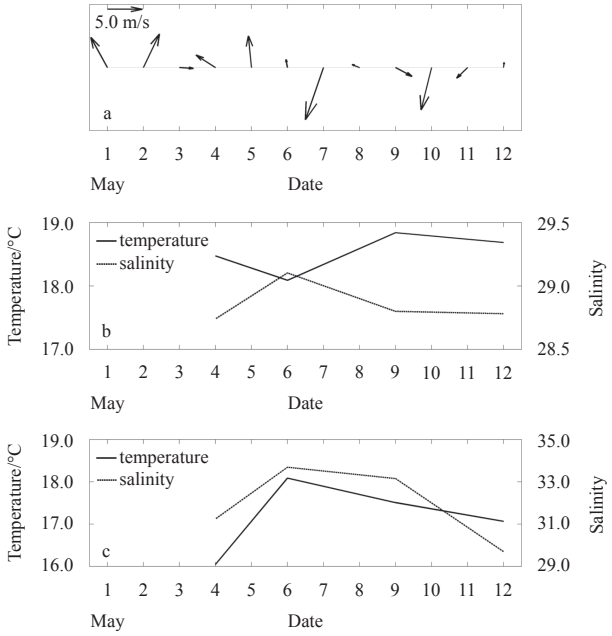

Fig. 6. Variations in daily wind vector data from ASCAT (a), temperature and salinity in the 3 m layer at Sta. B9 (b), and temperature and salinity in the 22 m layer at Sta. B9 (c).

5 Conclusions

The observational data of three sections off the central Zhejiang coast in the spring of 2016 were analyzed; and some good results of temperature, salinity and density in the survey area were obtained, providing a further understanding of the hydrography off the central Zhejiang coast in spring.

The distributions of thermohaline in the three sections show that the high temperature and low salinity water (i.e., the Zhe-Min Coastal Water) is distributed in the upper layer of the sections, and the high temperature and high salinity water (i.e., the inshore branch of TWCW) is distributed in the lower layer. Cold water patches were observed in the middle layer of sections distributed from 10 to 25 m, where isopycnals are dense (or halocline).

Upwelling was found at the upper part of Sta. B9. However, the strength was weak, and the duration was short. The TWCW climbing was found in all the three sections, but in a short period of time, the intensity of climbing changed and even disappeared.

Variations in the intensities of upwelling and TWCW climbing affect the formation, depth, thickness, strength, and disappearance of thermocline or halocline layer. When the upwelling outcrops to the surface layer, the thermocline or halocline layer disappears. When the TWCW climbing is strengthened, the depth of thermocline or halocline layer decreases, the thickness decreases, and the intensity increases; otherwise, the reverse occurs. The intensity of TWCW climbing in spring was still relatively weak and not strong enough to outcrop the thermocline or halocline barrier layer to reach the sea surface.

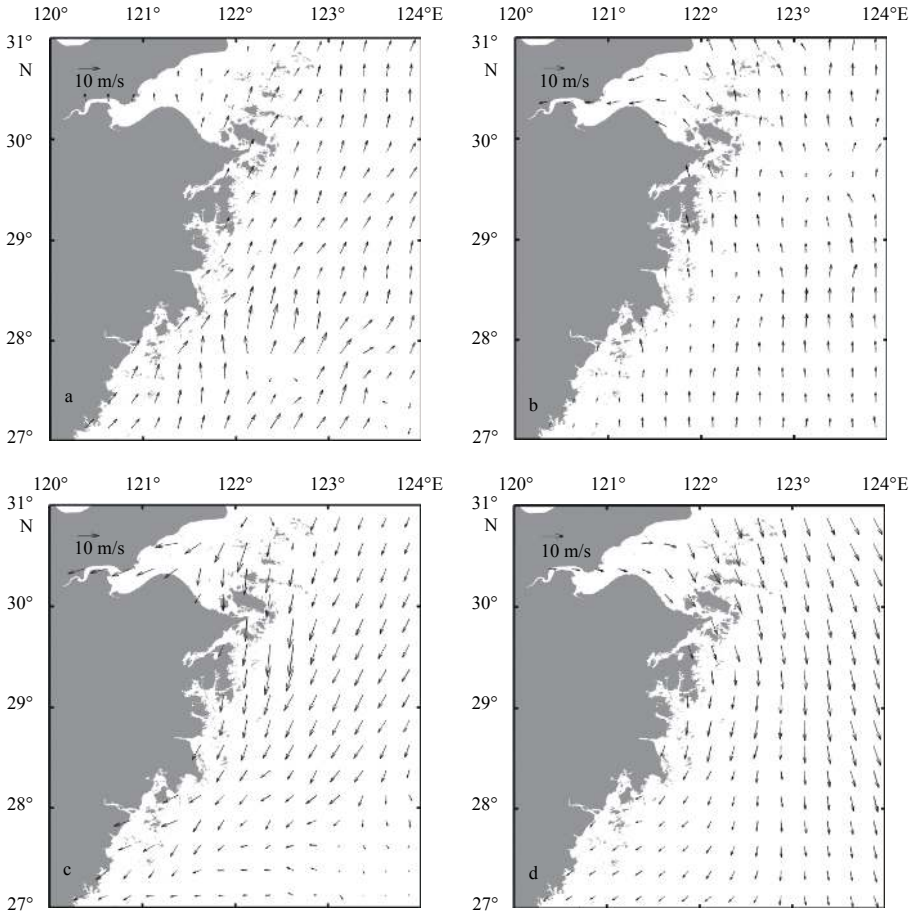

Fig. 7. Distribution of daily wind vector data from ASCAT. a. May 2, b. May 5, c. May 7, and d. May 10.

Combined with the wind field data obtained from ASCAT, we found that the intensity of upwelling corresponds well with the variation in wind. Upwelling is induced by southerly winds and strengthened if the southerly wind is continuous. When the wind turns into a northerly wind, the upwelling becomes weak and even disappears. However, the intensity of TWCW climbing is inconsistent with the wind variation.

References

Bai Tao, Yang Dezhou, Yin Baoshu. 2009. Numerical study of upwelling of the Changjiang River Estuary and its adjacent sea area in summer. Marine Sciences (in Chinese), 33(11): 65–72

Beardsley R C, Limeburner R, Yu H S, et al. 1985. Discharge of the Changjiang (Yangtze River) into the East China Sea. Continental Shelf Research, 4(1–2): 57–76, doi: 10.1016/0278-4343(85)90022-6

Hu Dunxin, Lv Lianghong, Xiong Qingcheng, et al. 1980. A study on upwelling about the coastal sea of Zhejiang. Science Bulletin (in Chinese), 25(3): 131–133

Hu Jiangyu, Wang Xiaohua. 2016. Progress on upwelling studies in the China seas. Reviews of Geophysics, 54(3): 653–673, doi: 10.1002/2015RG000505

Huang Rongxiang. 1996. Indication of existing Minzhong coast upwelling in winter. Marine Sciences (in Chinese), 2(1): 68–72

Huang Zuke, Yu Guangyao, Luo Yiyong, et al. 1996. Numerical modelling of tide-induced upwelling in coastal areas of the East China Sea. Journal of Ocean University of Qingdao (in Chinese), 26(4): 405–412

Li Hongmei, Shi Xiaoyong, Wang Hao, et al. 2014. An estimation of nutrient fluxes to the East China Sea continental shelf from the Taiwan Strait and Kuroshio subsurface waters in summer. Acta Oceanologica Sinica, 33(11): 1–10, doi: 10.1007/s13131-014-0550-2

Liu Xianbing, Su Jilan. 1991. Numerical study of upwelling and coastal fronts on the coastal sea of Zhejiang. Haiyang Xuebao (in Chinese), 13(3): 305–314

Lou Xiulin, Shi Aiqin, Xiao Qingmei, et al. 2011. Satellite observation of the Zhejiang Coastal upwelling in the East China Sea during 2007–2009. Proceedings of the SPIE 8175, Remote Sensing of the Ocean, Sea Ice, Coastal Waters, and Large Water Regions. Prague, Czech Republic: SPIE, 283–304

Lü Xingang, Qiao Fangli, Xia Changshui, et al. 2006. Upwelling off Yangtze River estuary in summer. Journal of Geophysical Research: Oceans, 111(C11): C11S08

Lü Xingang, Qiao Fangli, Xia Changshui, et al. 2007. Tidally induced upwelling off Yangtze River estuary and in Zhejiang coastal waters in summer. Science in China Series D: Earth Sciences, 50(3): 462–473, doi: 10.1007/s11430-007-2050-0

Luo Yiyong, Yu Guangyao, Huang Zuke. 1998. Numerical studies of upwelling in coastal areas of the East China Sea I—the tide induced upwelling. Acta Oceanologica Sinica, 17(1): 15–25

Mao Hanli, Gan Zijun, Lan Shufang. 1963. A preliminary study of the Yangtze diluted water and its mixing processes. Oceanologia et Limnologia Sinica (in Chinese), 5(3): 183–206

Ni Tingting, Guan Weibing, Cao Zhenyi, et al. 2014. Numerical study on the upwelling of Zhejiang coast in spring. Journal of Marine Sciences (in Chinese), 32(2): 1–13

Pan Yuping, Sha Wenyu. 2004. Numerical study on winter coastal upwelling off Fujian and Zhejiang coast. Oceanologia et Limnologia Sinica (in Chinese), 35(3): 193–201

Pan Yuqiu, Xu Duanrong, Xu Jianping. 1985. Frontal structure, variation and causes on upwelling of Zhejiang coast. Haiyang Xuebao (in Chinese), 7(4): 401–411

Pu Yong Xiu. 1983. A preliminary analysis about the mechanism of expand of the Yangtze River diluted in summer. Donghai Marine Science (in Chinese), 1(1): 43–51

Qiao F L. 2012. Regional Oceanography of China seas–Physical Oceanography (in Chinese). Beijing: China Ocean Press, 189–251

Qiao Fangli, Yang Yongzeng, Lü Xingang, et al. 2006. Coastal upwelling in the East China Sea in winter. Journal of Geophysical Research: Oceans, 111(C11): C11S06

Shi Xiaoyong, Li Hongmei, Wang Hao, et al. 2013. Taiwan Warm Current and its impact on the areas of frequent harmful alga bloom in the East China Sea in summer. Oceanologia et Limnologia Sinica (in Chinese), 44(5): 1208–1215

Song Shuqun, Li Zhao, Li Caiwen, et al. 2017. The response of spring phytoplankton assemblage to diluted water and upwelling in the eutrophic Changjiang (Yangtze River) Estuary. Acta Oceanologica Sinica, 36(12): 101–110, doi: 10.1007/s13131-017-1094-z

Tang Danling, Di Baoping, Wei Guifeng, et al. 2006. Spatial, seasonal and species variations of harmful algal blooms in the South Yellow Sea and East China Sea. Hydrobiologia, 568(1): 245–253, doi: 10.1007/s10750-006-0108-1

Wang Zongshan, Xu Bochang, Zou Emei, et al. 2002. Formation cause of the intermediate cold water in the northwesaern East China Sea. Advances in Marine Science (in Chinese), 20(3): 68–7

Wang Qing, Zhu Liangsheng, Wang Dongxiao. 2014. A numerical model study on multi-species harmful algal blooms coupled with background ecological fields. Acta Oceanologica Sinica, 33(8): 95–105, doi: 10.1007/s13131-014-0459-9

Wu Bin, Song Jinming, Li Xuegang. 2015. Distribution and chemical speciation of dissolved inorganic arsenic in the Yellow Sea and East China Sea. Acta Oceanologica Sinica, 34(6): 12–20, doi: 10.1007/s13131-015-0682-z

Xu Jianping. 1986. Preliminary analysis of the hydrologic structure in the coastal upwelling area off Zhejiang in winter. Donghai Marine Science (in Chinese), 4(3): 18–23

Xu Jindian, Huang Jiang, Qiu Yun, et al. 2015. Spatial structure characteristics of Zhejiang and Fujian coastal water and their evolution. Journal of Tropical Oceanography (in Chinese), 34(1): 1–7

Xu Bochang, Wang Zongshan, Zhou Emei, et al. 2000. The spatial and temporal variations of the characteristics of the intermediate cold water in the northwest of the East China Sea. Journal of Oceanography of Huanghai & Bohai Seas (in Chinese), 18(2): 1–7

Yang Dezhou, Yin Baoshu, Sun Junchuan, et al. 2013. Numerical study on the origins and the forcing mechanism of the phosphate in upwelling areas off the coast of Zhejiang province, China in summer. Journal of Marine Systems, 123–124: 1–18, doi: 10.1016/j.jmarsys.2013.04.002

Zeng Dingyong, Ni Xiaobo, Huang Daji. 2012. Temporal and spatial variability of the ZheMin Coastal Current and the Taiwan Warm Current in winter in the southern Zhejiang coastal sea. Scientia Sinica Terrae (in Chinese), 42(7): 1123–1134

Zhang Qilong, Liu Hongwei, Qin Sisi, et al. 2014. The study on seasonal characteristics of water masses in the western East China Sea shelf area. Acta Oceanologica Sinica, 33(11): 64–74, doi: 10.1007/s13131-014-0556-9

Zhou Feng, Xuan Jiliang, Ni Xiaobo, et al. 2009. A preliminary study on variations of the Changjiang Diluted Water between August 1999 and 2006. Haiyang Xuebao (in Chinese), 31(4): 1–12

Zhu Jianrong. 2003. Dynamic mechanism of the upwelling on the west side of the submerged river valley off the Changjiang mouth in summertime. Chinese Science Bulletin, 48(24): 2754–2758, doi: 10.1007/BF02901770